2017-03

Optimisation of focused wave group runup on a plane beach

Whittaker, CN

10.1016/j.coastaleng.2016.12.001
Coastal Engineering
Elsevier BV

Optimisation of focused wave group runup on a plane beach

C. N. Whittaker[a,*], C. J. Fitzgerald[c], A. C. Raby[b], P. H. Taylor[c], J. Orszaghova[d], A. G. L. Borthwick[e]

[a]*Department of Civil and Environmental Engineering, Faculty of Engineering, University of Auckland, Symonds St, Auckland 1010, New Zealand*
[b]*Department of Marine Science and Engineering, Faculty of Science and Engineering, Plymouth University, Drake Circus, PL4 8AA, UK*
[c]*Department of Engineering Science, University of Oxford, Parks Rd, Oxford, Oxfordshire OX1 3PJ, UK*
[d]*Centre for Offshore Foundation Systems, The University of Western Australia, 35 Stirling Highway, Crawley WA 6009, Australia*
[e]*School of Engineering, The University of Edinburgh, The King's Buildings, Edinburgh EH9 3JL, UK*

Abstract

Insight is provided into focused wave group runup on a plane beach by means of laboratory wave flume experiments and numerical simulations. A focused wave group is presented as an alternative to an empirical description of the wave conditions leading to extreme runup. Second-order correction to the laboratory wavemaker generation signal is observed to remove about 60% of the sub-harmonic error wave that would otherwise contaminate coastal response experiments. Laboratory measurements of the wave runup time history are obtained using inclined resistance-type wires and copper strips attached to the beach surface. The numerical wave runup model is based on hybrid Boussinesq-Nonlinear Shallow Water equations, empirical parameters for wave breaking and bed friction, and a wetting and drying algorithm. After calibration against experimental runup data, the numerical model reproduces satisfactorily the propagation, shoaling and runup of focused wave groups over the entire length of the wave flume. Results from a comprehensive parametric study show that both measured and predicted maximum runup elevations exhibit strong dependence on the linear focus amplitude of the wave group (linked to its probability of occurrence), the focus location, and the phase of the wave group at focus. The results also demonstrate that extreme runup events owing to focused wave incidence cannot be characterised using spectral parameters alone. The optimal band of focus locations shifts onshore as linear focus amplitude of the incident wave group increases. Optimisation of phase and focus location leads to a maximum runup elevation at each linear amplitude, and, when generated using second-order corrected paddle signals, the maximum runup appears to approach saturation

*Corresponding author
Email address: c.whittaker@auckland.ac.nz (C. N. Whittaker)

at very large focused wave amplitudes. This study therefore moves beyond simple wave focusing, and presents a focused wave group as a tool for investigating the relationship between extremes within an incident wave field and extreme wave runup.

Keywords: Runup, Focused wave groups, Wavemaker theory, Spurious error wave, Boussinesq numerical wave tank, Extreme waves

1. Introduction

Coastal communities rely on sea defence structures for protection against flood inundation. Worldwide, the populations of such communities are increasing, while much coastal defence infrastructure is ageing (ICE, 2014). Runup, the maximum elevation attained by seawater above the still water shoreline (Kobayashi, 1999), has a primary influence on surf-zone sediment transport, beach levels and coastal erosion (Ruggiero et al., 2001), wave overtopping of natural or artificial defence structures, and subsequent inland flooding. Storm-induced wave runup and its consequences are particularly sensitive to sea level rise (Penland et al., 2005; Dickson et al., 2007; Hall et al., 2006; Sutherland and Gouldby, 2003; Zhang et al., 2004) and climate variability (Ruggiero, 2013). Runup requires accurate estimation by coastal engineers and managers as part of routine coastal assessment studies.

Present understanding of wave runup on beaches and coastal structures is informed by field observations, physical experiments, and mathematical models. Such models and the empirical relationships derived from field/laboratory studies are used to predict extreme instances of runup. Runup and swash zone motions have been measured in field and laboratory campaigns using standard vertical wave gauges (e.g. Thornton and Guza, 1983; Kraus et al., 1994), non-intrusive altimeters (e.g. Blenkinsopp et al., 2016; Holman and Haller, 2013), inclined resistance-type wires (see Guza and Thornton, 1982; Raubenheimer et al., 1995; Holland et al., 1995; Hughes and Moseley, 2007, among many others), pressure transducers (e.g. Holman and Sallenger, 1985; Hughes and Moseley, 2007) and interpretation of video records (see Holman and Sallenger, 1985; Ruessink et al., 1998; Stockdon et al., 2006, among many others). More recently, lidar has been used for runup measurement in the field (Blenkinsopp et al., 2010; Almeida et al., 2013; Almar et al., 2014; Fiedler et al., 2015) and for measuring free surface elevations in certain large-scale experimental facilities (Blenkinsopp et al., 2012). A review of swash zone hydrodynamics, including the effects on beach morphodynamics, is provided by Brocchini and Baldock (2008).

Laboratory experiments allow testing of wave processes under controlled conditions, often considering propagation in one horizontal dimension within a wave flume (e.g. Mase and Iwa-

gaki, 1984; Mase, 1989; Kraus et al., 1994; Baldock et al., 1997; Erikson et al., 2005). Although the idealised geometries, relatively small model scales and simplified (regular or irregular) wave input typically used in laboratories may neglect certain physical processes observed in the field, laboratory experiments are useful tools for model validation and hypothesis testing. Numerical models often complement (and extend) laboratory or field experiments. Although recent advances in computational power have led to increasingly widespread use of advanced three-dimensional CFD models (such as the open-source OpenFOAM package, see Higuera et al., 2013, 2015), more computationally efficient solvers for simplified models are better suited to collect extreme statistics from large numbers of incident waves. Depth-integrated wave-resolving flow models (e.g. Erduran et al., 2005; Tonelli and Petti, 2012; Tissier et al., 2012; Shi et al., 2012) are able to describe pre- and post-breaking waves, achieving an effective compromise between computational efficiency and realistic representation of the dominant physical processes affecting wave runup. Soldini et al. (2013) found good agreement between their shallow-water model predictions and the empirical relationships of Stockdon et al. (2006) and Vousdoukas et al. (2009), and highlighted the effect of the beach profile on the maximum wave runup. Guza and Feddersen (2012) demonstrate the effect of directional spread and frequency characteristics on significant wave runup, and recommend both characteristics be included in parameterisations of infragravity wave runup.

A key runup-related design parameter is the extreme runup, often defined as the vertical elevation exceeded by the largest 2% of the runup excursions ($R_{2\%}$). This extreme runup is often treated empirically for broken incident waves, and has been characterised using the Iribarren number (see Hunt, 1959; Battjes, 1974):

$$\zeta = \frac{\beta}{(H/L_0)^{1/2}}, \tag{1}$$

where β is the beach slope, H the wave height and L_0 the deep-water wavelength. Different expressions involving the Iribarren number have been developed using laboratory experimental results (Hunt, 1959; Mase, 1989; van der Meer and Stam, 1992; Hedges and Mase, 2004). Hughes (2004) used the (maximum depth-integrated) momentum flux parameter to obtain an empirical relation for a range of slopes. Field data investigations also determined empirical relations between the offshore wave conditions/beach geometry (not exclusively using the Iribarren number) and $R_{2\%}$ (Guza and Thornton, 1982; Holman, 1986; Nielsen and Hanslow, 1991; Ruggiero et al., 2001; Stockdon et al., 2006; Vousdoukas et al., 2009). These empirical relationships, and others related to overtopping, form the basis of much coastal design (Pullen et al., 2007). Other stud-

ies on runup dynamics and swash spectra have been conducted by Raubenheimer et al. (1995); Raubenheimer and Guza (1996); Hughes and Moseley (2007); Hughes et al. (2010, 2014). Blenkinsopp et al. (2016) reviewed and assessed the applicability of the extreme wave parametisations in the context of the BARDEX *II* project (Masselink et al., 2016), finding that the bore height at collapse was an excellent predictor of the runup elevation in an irregular wave climate. Park and Cox (2016) used a Boussinesq model to derive an empirical formula to account for storm surge conditions and the presence of beach berms/dunes.

Wave focusing has been the subject of field, numerical and experimental investigations, particularly in the context of rogue wave formation (Kharif and Pelinovsky, 2003). Baldock et al. (1996) compared laboratory measured surface elevations and kinematics against linear theory and the second-order theory of Longuet-Higgins and Stewart (1960). Laboratory investigations by Johannessen and Swan (2001) demonstrated that directionality had a significant effect on wave group focusing, in agreement with previous numerical simulations by Johannessen and Swan (1997). Gibson and Swan (2007) analysed theoretical predictions of Bateman et al. (2001) to study changes in a wave spectrum near to a focusing event (in both unidirectional and spread sea states), and discussed the implications for rogue wave formation (see also Toffoli et al., 2010). Smith and Swan (2002) also highlighted the importance of nonlinearity and unsteadiness in numerical simulations of extreme focused waves. Sriram et al. (2015) considered the effect of linear and second-order generation signals on focused wave evolution in a parametric study within a physical wave flume. Sriram et al. (2015) found that spurious sub-harmonic free waves led to additional focus location shifts, and noted that the effect of such waves was likely to be greater for focus locations closer to the wavemaker.

This study seeks to determine the effectiveness of a focused wave group as a predictor of extreme runup on a plane beach (e.g. Hunt-Raby et al., 2011; Hofland et al., 2014). Instead of representing the incident field as a parameter (such as the significant wave height or period), this approach generates a compact wave group representing an extreme event within the incident wave field (see Jonathan and Taylor, 1997; Tromans et al., 1991; Walker et al., 2004, for offshore engineering applications) and determines the associated runup. The use of a compact wave group provides information on the physical processes generating extreme runup, and a means for the assessment of the possibility of runup saturation. This concept has been discussed by Raubenheimer and Guza (1996); Stockdon et al. (2006); Senechal et al. (2011), who found that saturation may occur in the frequency band associated with the incident wave spectrum but not in the lower-frequency band associated with infragravity waves. Given that an isolated

focused wave group is unlikely to generate free as opposed to bound infragravity waves until breaking occurs, the runup may be expected to saturate for high incident focused wave group amplitudes. This method may provide a complementary approach to existing empirical methods for determining extreme wave runup.

We use the linear NewWave profile of Tromans et al. (1991) as the input focused wave group for an experimental/numerical study into extreme wave runup on a plane beach. In NewWave theory a probabilistic analysis shows that the expected local shape of a large wave in a random sea state is the autocorrelation function, i.e. the Fourier Transform of the power density spectrum for the random sea state. NewWave theory was first validated using field data (from wave staff, downward pointing laser and radar rangefinders) from deep water locations where the necessary/underlying assumption that linear frequency dispersion is the dominant process affecting wave transformation is clearly true. NewWave validation at intermediate depth locations has also been demonstrated (Taylor and Williams, 2004). Recent analysis of field data from wave buoys by Whittaker et al. (2016) has demonstrated that NewWave could represent the average shapes of large storm waves observed in shallow water of depth $kD < 0.5$. This is a powerful result, demonstrating that even in shallow water depths the average shape of the largest event is a property of all the waves in the sea state (i.e. the autocorrelation function).

The target NewWave free surface elevation time series of the focused wave group is given by the linear superposition of wave modes:

$$\eta(x,t) = \frac{A}{\sigma^2} \sum_{i=1}^{N} S_{\eta\eta}(\omega_i) \cos(k_i(x - x_f) - \omega_i(t - t_f) + \phi)\Delta\omega, \tag{2}$$

where σ is the standard deviation of the sea state (with an associated variance $\sigma^2 = \sum S_{\eta\eta}(\omega_i)\Delta\omega$ in this discretised form), $S_{\eta\eta}$ is the power spectral density and ω_i is the angular frequency corresponding to the wavenumber k_i. A Pierson-Moskowitz spectrum with a peak frequency of $f_p = 0.464$ Hz, corresponding to a kD value of 0.71 for the offshore water depth $D = 0.5$ m, is adopted in the experimental/numerical focused wave study reported herein. The focusing event (x_f, t_f) is the spatial and temporal position/instant at which the wave group is in its most compact form according to Equation 2, which applies the linear dispersion relation for a constant water depth D (allowing calculation of the required paddle signal to generate the focusing event). It is important at this point to clarify the difference between the phase of each Fourier component and the overall shape of the focused wave group. A single frequency component of an irregular sea state would have the form $a_i \cos(k_i x - \omega_i t + \phi_i)$, where ϕ_i is the phase of each wave component

randomly chosen from a uniform phase distribution on $(0, 2\pi)$. However, in formulating a focused wave group this phase is not random, and can be expressed in terms of the phase of the entire wave group in the form $\phi_i = -k_i x_f + \omega_i t_f + \phi$, where (x_f, t_f) is the focusing event and ϕ is the phase of the wave group at focus. Hence, the frequency-independent phase of all the wave components ϕ is distinct from the focusing of the group; this phase which determines the position of the individual waves within this group. The energy concentration within the group for any value of ϕ is independent of the value of ϕ, this is related to the envelope of the group which may conveniently be taken as that for the crest-focused case of $\phi = 0$. Thus, we can talk about crest-focused, trough-focused and up- and down-crossing events, all with the same envelope.

The work of Smith and Swan (2002) has demonstrated the importance of nonlinearity on the focusing of wave groups in a range of uniform water depths. However, it should be noted that the creation of a perfectly focused wave group on a sloping beach is not the objective of the present work (particularly since breaking on the slope will prevent complete focusing of the large-amplitude waves of greatest interest). Instead, the wave group will be generated offshore with a given linear focus amplitude A and focus location x_f (i.e. where the Fourier components of the wave group come into phase ϕ), based on linear focusing in a constant water depth to that point. The wave group itself will evolve (nonlinearly) as it propagates up the slope, generating a maximum runup event. These nonlinear dynamics will be captured within the physical experiments and numerical model described in Sections 3 and 4 respectively. Thus, the dependence of runup on the input parameters A, x_f and ϕ may be determined without requiring a paddle signal specifying a nonlinearly-focused wave group at location x_f. Indeed, this description allows the focus location to be specified onshore of the breaking point and even the still water level (as discussed in Section 5), allowing a broader parametric study to be conducted than would be possible for nonlinearly focused wave groups on a slope. The amplitude A may be associated with a given probability of occurrence of this event in this sea state, based on Rayleigh statistics for a given number of waves (see Section 5.4). Thus, the use of a focused wave group allows determination of the runup of a wave with a given probability of occurrence (e.g. the largest wave in a storm containing N waves), providing a link with the runup generated by irregular sea states of different durations.

Although the application of the focused NewWave group to runup on a plane beach is the primary objective of this study, recent numerical simulations by Orszaghova et al. (2014) have demonstrated that any runup investigations conducted using a linear wave generation signal would be contaminated by a sub-harmonic error wave (see Schäffer, 1996). This was also identified

as an issue in previous experimental studies (Borthwick et al., 2006; Hunt-Raby et al., 2011). The removal of this error wave is therefore a secondary objective of the present work. The paper is structured as follows. Section 2 describes the application of the second-order wave generation theory of Schäffer (1996) to the experimental wavemaker, and the effectiveness of the error wave removal. Section 3 describes the experimental measurement of time-varying wave runup on a plane beach. Section 4 discusses calibration of the coupled Boussinesq-nonlinear shallow water (NLSW) equation solver. Section 5 demonstrates the effect of linear and second-order wave generation on the maximum experimental and numerical runup of focused wave groups.

2. Second-order (difference) correction of focused wave groups using piston-type wavemaker

Whenever a linear wave generation signal is used to create a focused wave group, spurious waves are created by the mismatch between the required super-harmonic and sub-harmonic bound waves (arising from interactions between the first-order components) and the boundary condition at the wavemaker, also including departures of the wavemaker from its mean position. Schäffer (1996) derives the full second-order generation theory required for a piston wavemaker to suppress spurious sub-harmonic and super-harmonic waves and obtains a wave field correct to second-order (corresponding to the formulation of Sharma and Dean, 1981, for waves propagating away from the paddle). More recent work has been conducted by Spinneken and Swan (2009a,b) for wavemakers operated in force-control mode. Successful elimination of the sub-harmonic error wave is crucial when investigating the runup or overtopping of extreme waves, as highlighted by Orszaghova et al. (2014). In this section, we describe an application of the theory of Schäffer (1996) to the experimental wavemaker, the practical limitations of this approach in our experiments and the implications for the subsequent experimental runup measurements.

The experiments were conducted in the wave flume of the COAST (Coastal, Ocean and Sediment Transport) Laboratory at Plymouth University, UK, in which waves were generated using an Edinburgh Designs Ltd (EDL) piston-type paddle. The laboratory flume, shown in Figure 1, was 35 m in length, 0.6 m in width and contained a 1 : 20 plane beach occupying approximately half its length. The beach comprised 12 mm thick smooth polypropylene panels, of average roughness $R_a = 0.11$ μm, attached to a stainless steel frame. The working depth in the horizontal section offshore of the beach was 0.5 m, and the beach toe was located 15.176 m from the wavemaker. Focus locations in this study are reported relative to the beach toe. To measure free surface elevation, twelve resistance wave gauges were mounted along the flat bed and along

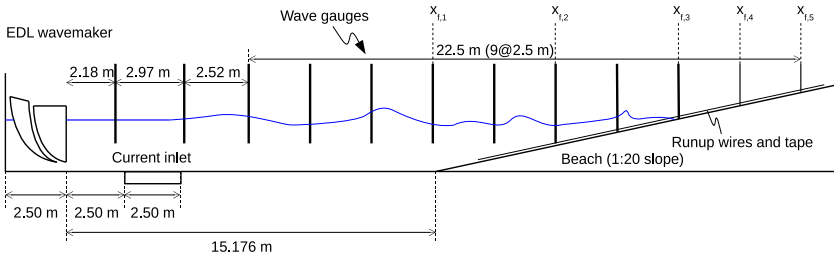

Figure 1: COAST laboratory flume containing the plane beach used for the runup experiments of the ENFORCE project.

the sloping beach within the flume at 2.5 m intervals The first three gauges had slightly different spacing, as seen in Figure 1.

The EDL wavemaker comprised two curved elements with a flat front face, with small gaps at the sides and base elements. This geometry avoids resonant amplification of water behind the wavemaker. However, the wavemaker could not be operated in pure displacement control due to software constraints (unlike the wavemaker used by Sriram et al., 2015), but needed to be controlled using target free surface elevations (prescribed an arbitrary distance from the wavemaker) and an appropriate transfer function. The lower frequency limit for piston paddle motions restricted the ability of the wavemaker to synthesise the full second-order sub-harmonic paddle signal correction. In these experiments, accurate Fourier representation of a given target long wave (incorporating the wavemaker transfer function to yield paddle motions) used a low frequency limit of $f = 0.03125$ Hz. Although not restrictive for linear wave generation in a typical wave tank with depths of O(1 m), the lower frequency limit does prove restrictive where the generation of a sub-harmonic correction wave is required to eliminate the spuriously generated long wave crest is required, i.e. second-order irregular wave or focused wave group generation.

Figure 2 illustrates the theoretical and experimental linear and second-order correction paddle displacements for a crest-focused wave group, with focus location at the beach toe. The theoretical displacements are calculated from the theory of Schäffer (1996). In the absence of pure displacement control for the laboratory wavemaker, second-order error wave suppression was approximated by adding a correction term to the target linear free-surface elevation supplied to the EDL software. This second-order correction should have eliminated the spurious free waves arising during linear wave generation. However, although the experimental and full theoretical correction paddle displacements are qualitatively similar, the slow pullback of the paddle necessary to eliminate the spurious long wave 'hump' created by the linear paddle motion

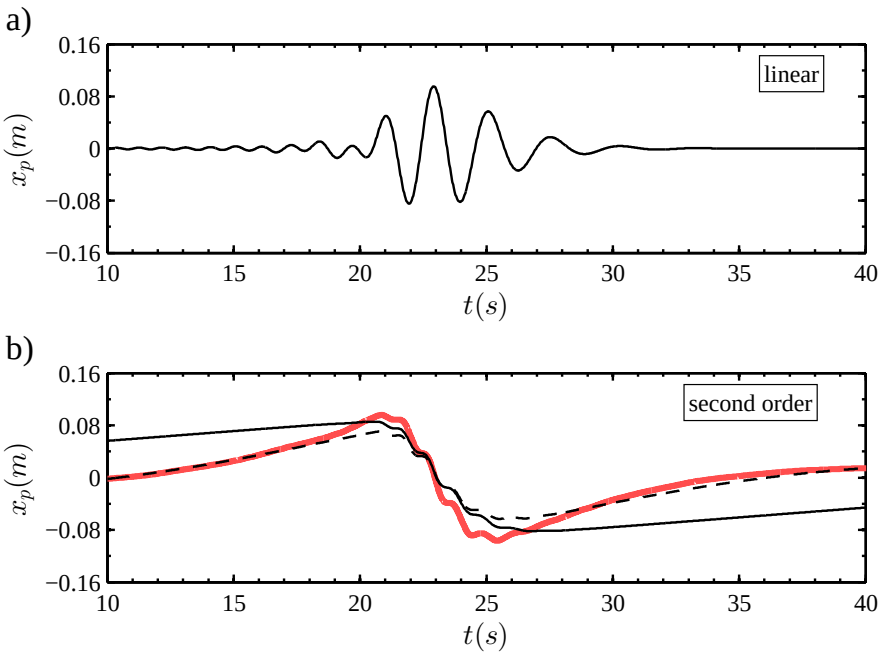

Figure 2: a) Linear and b) second-order paddle displacement time-histories from the laboratory wavemaker (thick red line) and for an idealised piston wavemaker (second-order signal obtained from the theory of Schäffer (1996)) using full (black) and partial second order generation (black, dashed) for a crest-focused wave group ($\phi = 0°$) of linear focus amplitude $A = 0.0855$ m focusing at the beach toe ($x_f = 0.0$ m).

could not be accurately synthesised. Two factors contributed to the experimental-theoretical paddle signal discrepancy: the different transfer functions and the low frequency limit for the experimental paddle motions. Therefore, long error wave suppression was only partially achieved in the laboratory.

The level of suppression of spurious long waves using the approximate method implemented for the EDL wavemaker in the COAST laboratory wave flume is now assessed with reference to a fully nonlinear numerical wave tank (NWT) incorporating a moving boundary piston wavemaker and a constant water depth. This fully nonlinear potential flow (FNPF) model, developed by Bai and Eatock Taylor (2006, 2007), provides an ideal numerical benchmark for assessing nonlinear wave generation in that there are no further assumptions regarding either frequency dispersion or wave nonlinearity beyond those of potential flow. (The Boussinesq-nonlinear shallow water equation model, which is used in all subsequent sections to simulate focused wave runup on the beach, assumes that weakly nonlinear, weakly dispersive waves propagate in the region outside the breaker line.) To assess the performance of the laboratory wave generator, measured and

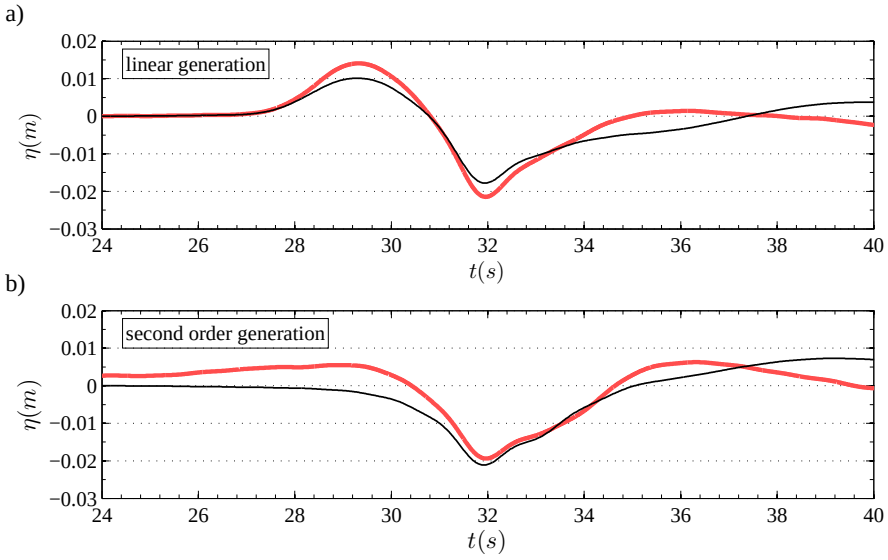

Figure 3: Comparison between second-order sub-harmonic components of the free-surface elevation at focus for wave groups of linear focus amplitude $A = 0.0855$ m, focus location $x_f = 0.0$ m and phase $\phi = 0°$ generated using first-order and second-order corrected paddle signals in the physical experiments (red line) and fully nonlinear potential flow (FNPF) model (thin black line).

FNPF-predicted free surface elevation time histories are compared for linear-focused wave groups propagating over the flat bed portion of the laboratory wave tank, focusing at the beach toe. Beach reflections, present in the laboratory tests but absent from the constant-depth FNPF simulations, are small relative to the amplitude of the compact wave group at focus, particularly during the propagation of the most significant crests and troughs. Harmonic decomposition of the free-surface elevation signals, necessary to isolate linear and second-order sub-harmonic components of the total wave, was achieved using the phase manipulation method of Fitzgerald et al. (2014) based on the fourth-order Stokes expansion.

Discrepancies of over 10% in the first harmonic free wave were found between the model and experimental results for the two intermediate linear focus amplitudes. Scale factors were applied to the linear paddle signals in the numerical simulations, with a corresponding quadratic increase to the second-order corrections. Both the FNPF and Boussinesq-NLSW models employed this scaling when simulating the laboratory focused wave groups.

Figure 3 presents time histories of the measured and predicted second-order sub-harmonic components of the free-surface elevation at the beach toe focus location, for both linear and second-order corrected wave generation of a crest-focused wave group of amplitude $A = 0.0855$ m.

Although not shown, the agreement between predicted (having applied the appropriate scale factor to the paddle signal) and measured first harmonic is excellent for both linear and second-order corrected paddle signals. However, the second order sub-harmonic time-histories show that the spurious long wave which precedes the main sub-harmonic bound wave trough is reduced in amplitude but not eliminated from the experiments. A reduction of approximately 60% in the sub-harmonic error wave amplitude has been achieved. Recently Sriram et al. (2015) found good agreement between theory and measurements for second-order corrected wave groups in a long flume with centre frequencies of 0.68 Hz and 1.08 Hz; the experimental wave groups in the present study may be considered to be an intermediate case between those generated by linear paddle signals and the fully-corrected groups reported by Sriram et al. (2015). In the experimental test, the long error wave travelling in front of the main linear wave train appears to be smeared, most likely due to lack of very low frequency motions by the paddle wavemaker. Nevertheless, we conclude that application of the Schäffer (1996) correction to the EDL piston wavemaker has proven to be reasonably successful in suppressing the second-order error waves, and in particular, the long error wave. The results of Orszaghova et al. (2014) imply that the runup measured in the physical experiments will be artificially increased compared to that predicted by the numerical model. The results shown in Section 5 are consistent with this implication. Additionally, the actual focus location may be shifted in the onshore direction by the residual sub-harmonic error wave (Sriram et al., 2015).

3. Laboratory measurement of time-varying runup

Time-varying runup was measured using resistance-type probes mounted parallel to the plane beach (Guza and Thornton, 1982; Raubenheimer et al., 1995; Holland et al., 1995; Hughes and Moseley, 2007). Two sets of stainless steel wires were mounted 5 mm and 10 mm above the beach surface. Additionally, two strips of copper tape (5 mm width, 20 mm spacing) were adhered to the beach surface to act as a zero-elevation resistance-type probe. Figure 4 shows the different devices used to obtain measurements within the swash zone. The wave gauges, wire and tape operated at a recording frequency of 128 Hz. Based on the effects of surface tension and their calibration, the runup wires and copper tape have a reduced accuracy of approximately ± 2 mm in the vertical direction.

The wires and tape served different functions. Previously, Holland et al. (1995) observed that a wire elevated above the beach surface could measure a reduced maximum runup elevation and respond more rapidly to the start of the rundown (due to the changing curvature of the

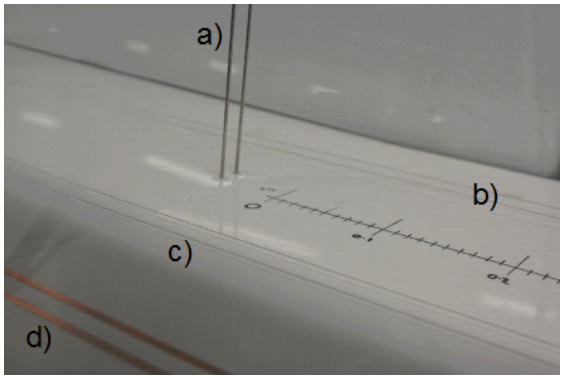

Figure 4: Close-up photograph of measurement devices located in the swash zone, including (a) a vertical resistance-type wave gauge embedded in the beach, (b) a pair of stainless steel wires at 10 mm elevation above the beach, (c) a pair of stainless steel wires at 5 mm elevation above the beach, and (d) two strips of copper tape adhered to the beach surface.

free surface during runup and rundown events). However, water pooling on the surface of the shallow slope means that an elevated sensor would be relatively less affected by surface tension than a sensor on the beach surface. Figure 5 illustrates the effect of elevation above the beach surface on the runup time series measured by the two sets of elevated wires and the copper tape. As expected, the maximum runup measured by the copper tape on the beach surface is larger than that measured by either of the wires. The tape did not capture rapid changes in shoreline elevation (e.g. at approximately 36 s), and responded to rundown more slowly due to surface tension acting on the beach surface. The 5 mm elevated wire was somewhat less sensitive to rapid variations in shoreline elevation than the 10 mm elevated wire (e.g. at approximately 33 s) due to surface tension effects. Thus, measurements obtained by the 10 mm elevated wire are used for time series comparisons with the numerical model predictions in Section 4, and measurements by the copper tape are used to record maximum runup. It should also be noted that lateral variations in the runup flow (due to the three-dimensionality of the wave breaking process) may lead to additional differences between the time series recorded by the different measurement devices. These lateral variations will be most severe for the largest incident wave amplitudes, where more violent wave breaking will lead to highly turbulent runup flow.

In summary, the COAST Laboratory experiments provide a dataset of both the time variation (using the elevated wires) and the maximum elevation (using the copper tape) of focused wave runup on a plane beach. (This dataset can be obtained upon request from Dr A. C. Raby at Plymouth University or from the first author.) These data provide an improvement over

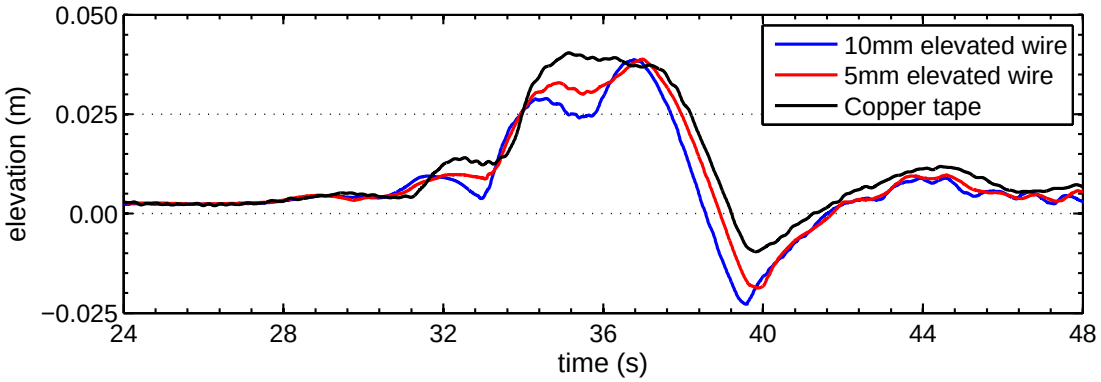

Figure 5: Runup time series recorded by the two elevated wires and the copper tape, illustrating the effects of wire gauge elevation and surface tension on the runup measurements.

observations of the maximum elevation only, allowing more robust calibration of the numerical model. The free surface elevations recorded by the wave gauges and the runup time series recorded by the 10 mm wire will be used for this calibration in the next section.

4. Calibration of model breaking and friction parameters using experimental data

Focused wave group runup in the laboratory wave flume is numerically simulated using a 1-D hybrid Boussinesq-NLSW equation model (OXBOU). Breaking is modelled approximately by locally switching from the Boussinesq to the NLSW equations. Switching between the two sets of equations simply involves retaining or neglecting the dispersive Boussinesq terms. However, the numerical solution method must switch from finite difference methods for the Boussinesq flows to shock-capturing finite volume methods for the NLSW flows and so careful treatment of the solution methods at this transition are necessary (c.f. Orszaghova, 2011). Breaking is assumed to occur if the free-surface slope exceeds a prescribed threshold value ($-\eta_x > 0.4$) corresponding approximately to a front face slope of 22°. The transition zone occupies half a wavelength, commencing one quarter of a wavelength offshore of the most offshore point where the breaking criterion is satisfied. Within the transition zone, the Boussinesq terms are ramped down to zero. Inshore of the transition zone the broken waves are modelled as bores using the NLSW equations. The breaking location is recalculated at every time step and tracks the breaking waves inshore until breaking occurs further offshore. Full details of the model formulation are provided by Orszaghova et al. (2012). The threshold front face slope of 22° has yielded excellent agreement with laboratory measurements for runup of solitary waves and steep wave groups on

beaches with slopes less than or equal to 1:20 (Orszaghova, 2011).

The location of the moving shoreline in OXBOU is defined as the most shoreward position where the water depth drops below a prescribed value (1 mm by default). Similarly, the runup location measured by the elevated runup wires corresponds to the most shoreward point where the water depth equals the wire elevation above the bed, here approximately 5 mm and 10 mm. Satisfactory agreement should therefore be possible between model (modifying the default 1 mm minimum water depth) and experiment. However, surface tension retarded the swash flow on the smooth beach in the laboratory experiments. Although no surface tension term is included in the NLSW equations, the friction coefficient C_f scaling the bed friction force ($\tau_b = \rho C_f u|u|$) was tuned to the approximate effect of surface tension. This corresponds to Chézy's roughness coefficient of almost 31 $\mathrm{m}^{1/2}s^{-1}$ or Manning's roughness coefficient of 0.02 $\mathrm{sm}^{-1/3}$ in water of depth 0.05 m.

This value of the friction coefficient is therefore somewhat larger than is expected for smooth plastic material such as polypropylene - typical values of $0.009 - 0.011$ $\mathrm{sm}^{-1/3}$ are quoted for Manning's roughness coefficient for plastic. However, calculations based on Manning's formula often assume uniform flow where the majority of energy dissipation is caused by surface roughness. In the case of wave runup on a sloping beach (with a much steeper slope than observed in standard open-channel flow situations), the additional energy dissipation by turbulent wave breaking may account for the larger apparent roughness required here. Additionally, bed friction forces are relatively larger in water of smaller depth and were only observed to have a significant effect at the swash edge, much like surface tension. In the absence of a more sophisticated treatment of surface tension, an artificial increase of bed friction was considered an adequate substitute.

Figure 6 shows a preliminary comparison of experimental and numerical free surface elevation time histories including the generation, propagation, shoaling, breaking and runup on a plane beach of a compact focused wave group. This follows a similar model calibration approach used by Raubenheimer et al. (1995) and Kobayashi and Wurjanto (1992). The wave breaking criterion was $s = -\eta_x^c = 0.4$ and bed friction coefficient was $C_f = 0.008$, using default values suggested by Orszaghova et al. (2012). The empirical scaling factor for the wavemaker motions was applied to each component of the theoretical linear input paddle signal. Following grid convergence tests, the grid spacing was $\Delta x = 0.01$ m and the time step was $\Delta t = 1/256$ s (for this and all subsequent focused wave runup simulations reported herein). Despite not optimising the two tuning parameters, the agreement between model and experiment appears to be satisfactory. It

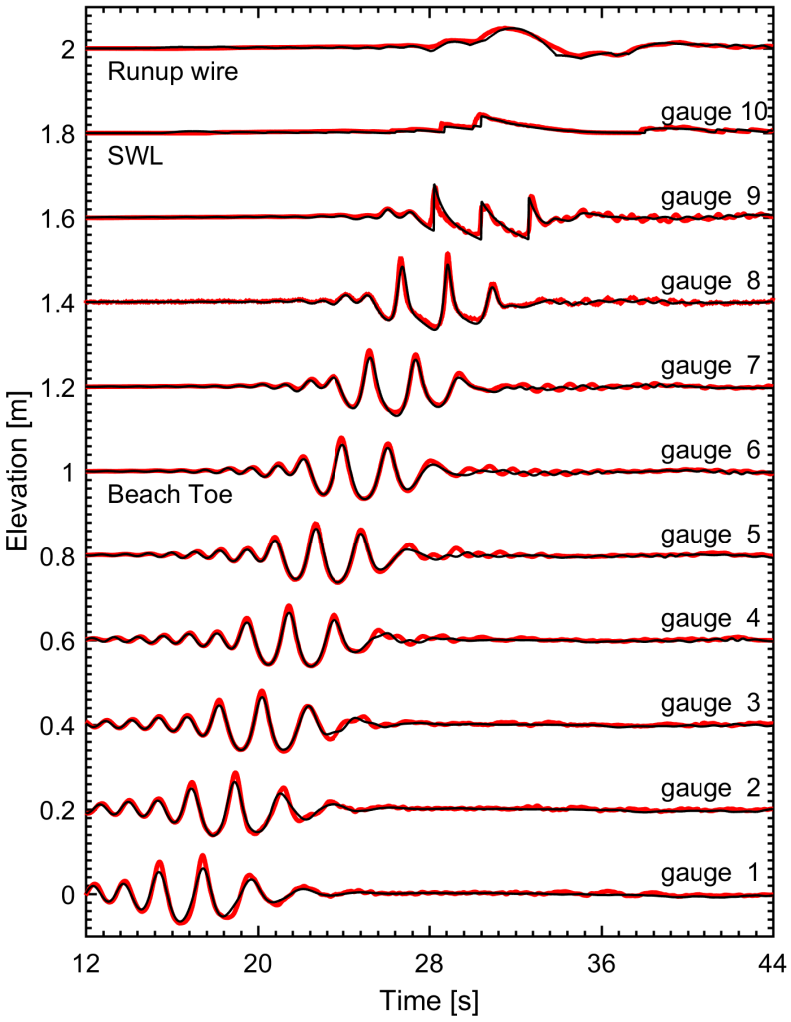

Figure 6: Free-surface elevation time histories of a typical focused wave group, as measured by ten wave gauges and the 10 mm runup wire (red) and as computed by OXBOU (black).

is clear that the shoaling, wave breaking, bore motions at the still water shoreline and runup (using the 10 mm elevated wire) were captured very accurately by the model.

It should be noted that the second-order paddle signals described in Section 2 focused on the elimination of the sub-harmonic error wave, identified by Orszaghova et al. (2014) as having the greatest impact on the runup elevations. The large high-frequency content in the experimental measurements recorded after the focusing event is due to residual superharmonic error waves, which are not present in the model predictions. This is also the reason for the larger high-frequency content observed in the wave gauge signals shown in Figure 7. These superharmonic error waves have a negligible effect on the maximum runup elevation, since they arrive at the beach well after the focused wave group. The model slightly under-estimates the maximum amplitude of the crests within the focused wave group, due to the assumption of weak nonlinearity in the Boussinesq equations (Orszaghova et al., 2012). However, this slight under-estimation does not significantly affect the subsequent agreement between the model and experiment.

Figure 7 shows the effect of altering the wave breaking parameter s from 0.4 to 0.5, on bore motions at Gauge 9 and 10 and shoreline motions, as measured by the runup wire 10 mm above the beach, for a focused wave group with focus location $x_f = 12.5$ m, phase at focus $\phi_f = 165°$ and focus amplitude of $A = 0.0855$ m. This linear amplitude was used to nondimensionalise the amplitudes and runup elevations. The larger value of wave breaking parameter ($s = 0.5$) leads to significant overestimation of bore height (at the vertical gauges) and shoreline motions. The laboratory measurements from Gauge 10 indicate that a small secondary bore just reaches the still water shoreline at $t = 33$ s. Depending on the threshold free-surface slope for breaking, the numerical model predicts that this secondary bore either does not reach still water shoreline ($s = -\eta_x^c = 0.4$) or that a much larger secondary bore reaches the still water shoreline ($s = -\eta_x^c = 0.5$). A larger bore is predicted for at higher s for two reasons: first, the initial bore height is greater because further shoaling of the wave crest occurs; and second, the dissipation of energy captured by the NLSW equations starts to act further inshore for the larger threshold breaking slope. For this reason, choice of $s < 0.4$ is unlikely to provide better agreement with experimental measurements and so $s = 0.4$ is used in all the following simulations. Agreement between prediction and measurement of the moving shoreline is improved by choosing a slightly larger bed friction coefficient $C_f = 0.01$ than would be expected for such a smooth beach (the default value $C_f = 0.008$ recommended by Orszaghova et al. (2012) is for a cement floor beach of similar dimensions).

It is evident from the comparisons with the 10 mm elevation runup wire measurements in

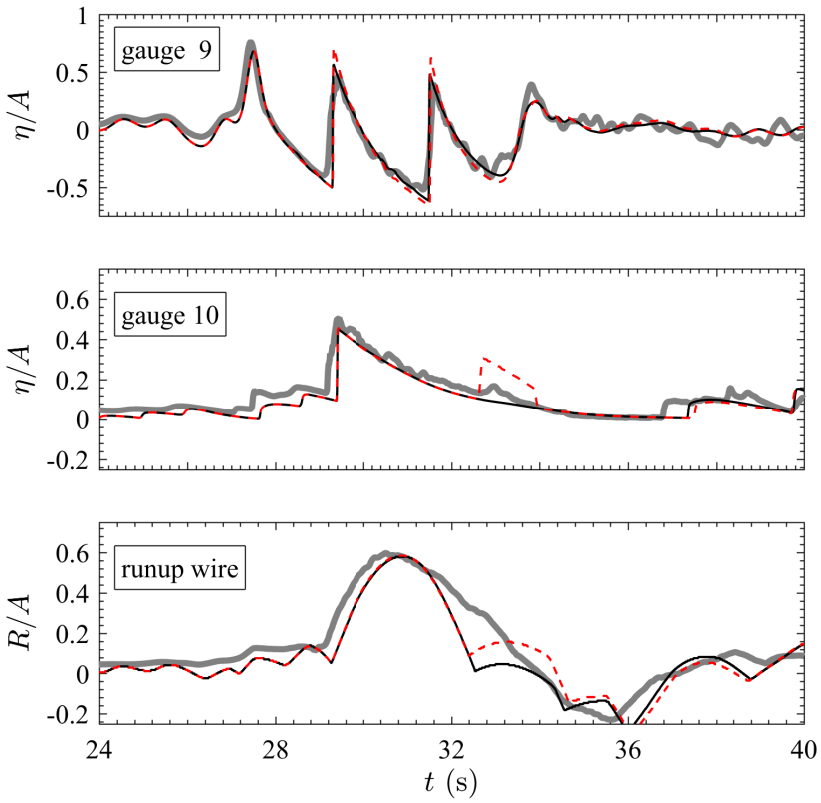

Figure 7: Free-surface elevations and vertical runup time-histories (from runup wire 10 mm above beach) of a focused wave group yielding large wave runup (amplitude $A = 0.0855\,\mathrm{m}$, focus location $x_f = 27.676\,\mathrm{m}$, phase at focus $\phi = 165°$), generated with a second order corrected paddle signal, as measured experimentally (grey) and predicted by OXBOU for threshold local surface slope 0.4 (black) and 0.5 (red, dashed). Wave amplitudes and runup elevations have been nondimensionalised by the linear focused wave amplitude A.

Figure 7 that the motion of the time-varying 'shoreline' (the location, in the plane of the beach face, shoreward of which the water depth is less than 10 mm) is slightly over-predicted by the numerical simulations. It should of course be noted that the numerical model does not account for surface tension, 3-D effects, non-hydrostatic pressure, and aeration, all of which become highly important in the free surface motions occurring at the air-water-beach interface. The lack of retarding surface tension in the model helps to explain the larger high-frequency content in the numerical predictions of the moving shoreline (measured experimentally using the runup wire), despite the larger high-frequency content in the experimental gauge measurements (due to the superharmonic error waves). Agreement between numerical prediction and experiment at the still water shoreline gauge (Gauge 10) is observed to be excellent.

5. Extreme runup of focused wave groups

5.1. Parametric dependence of extreme runup events

We now consider extreme runup elevations generated by focused wave groups, and the conditions contributing to these extreme runup elevations. Using numerical simulations, Orszaghova (2011) investigated the dependence of the maximum focused wave group runup on the linear focus amplitude, linear focus location and phase of the group at focus on a beach of slope 1:20. The flume geometry and focused wave driving conditions matched those of previous laboratory tests undertaken at the U.K. Coastal Research Facility and reported by Hunt (2003). This geometry is also adopted in the current study (see Figure 1). A parametric investigation, resembling that undertaken numerically by Orszaghova (2011), is conducted experimentally using the approximate second-order wave generation described in Section 2 and the runup measurement techniques discussed in Section 3. Runup values predicted by the calibrated hybrid Boussinesq-nonlinear shallow water equation solver (using full second-order generation) are then compared to the corresponding measurements.

The focused waves considered in this parametric study are derived from a Pierson-Moskowitz spectrum with a spectral peak at a frequency of 0.464 Hz and a high-frequency cut-off of 2.0 Hz. Based on Equation 2, the parameters varied during these experiments were the linear amplitude of the wave group at focus A, the focus location x_f and the phase of the wave group within its envelope at the focus location ϕ. Focus is defined here as the location in both space and time when the wave group acting under linear dispersion on constant depth is most compact. Figure 1 shows the selected focus locations. Table 1 summarises the parameters tested during the physical

Parameter	Experimental values
A (m)	0.0285, 0.0570, 0.0855, 0.114
x_f (m) relative to the paddles	15.176, 20.176, 25.176, 27.676, 30.176
relative to the beach toe	0, 5, 10, 12.5, 15
relative to the shoreline	-10, -5, 0, 2.5, 5
ϕ (degrees)	15, 30, ... 345, 360

Table 1: Values of linear wave group amplitude at focus A (used to nondimensionalise the runup elevations), focus location x_f (relative to the beach toe) and wave group phase at focus ϕ investigated experimentally.

experiments. Although the simulations of Orszaghova (2011) also included focused wave groups with linear focus amplitude of 0.1425 m, these experiments required a larger paddle sweep than could be produced by the laboratory wavemaker. Thus, the largest amplitude tested was 0.114 m. The runup elevations reported in this section were nondimensionalised by the amplitude A. The focus locations ranged from the toe of the beach to ~ 5 m beyond still water shoreline (SWS). A total of 480 focused wave runup tests (employing second-order corrected paddle signals) were conducted during the parametric study. As noted by Orszaghova (2011), the concept of a focus location far up the beach (i.e. beyond SWS) may seem counter-intuitive, since interactions with the beach would render the waves unable to reach the target location. However, the focus location merely controls the relative phasing of the different frequencies within the wave group on the constant depth region offshore of the beach toe. As stated in Section 1, the focus location is used as a parameter controlling the properties of the compact wave group, rather than as a target location on the beach for a nonlinearly-focused wave group.

This section initially examines the focused wave group properties which contribute to the maximum and minimum runup values for a subset of the full parameter space, extending the analysis of Orszaghova (2011). Full second-order corrected numerical model results are used, to avoid contamination by the sub-harmonic error wave. All groups considered have a linear focus amplitude $A = 0.0855$ m, and runup is again nondimensionalised by this amplitude. The best agreement between model and experiment was achieved for $A = 0.0855$ m. Table 2 lists the focus locations and phases of three 'optimised' (x_f and ϕ combinations generating maximum runup) groups with this amplitude.

Figure 8 shows the free surface elevation time series for the three optimised wave groups at the beach toe, SWS, and moving shoreline, all shifted so that the maximum runup occurs at $t = 0$. Note that the times have been nondimensionalised by the peak angular frequency of the

Focus location (m)	R_{max} (m)	Phase for R_{max} (°)	R_{min} (m)	Phase for R_{min} (°)
7.5	0.075	60	0.040	195
10.0	0.078	330	0.040	120
12.5	0.075	255	0.045	60

Table 2: Focus locations and phases at focus leading to the maximum/minimum runup of focused wave groups with $A = 0.0855$ m, where the focus locations are expressed relative to the beach toe.

incident Pierson-Moskowitz spectrum $\omega_p = 2\pi f_p$. The runup curves are strikingly similar. The (time-shifted) free surface elevations are almost identical at the SWS and the beach toe. All three records resemble a trough-focused wave group at the beach toe at approximately $\omega_p t \sim -23$, or $t \sim 8$s before the time of the maximum runup. The waves appear to have broken between the beach toe and SWS, and the waves recorded at the SWS have the saw-toothed shape typical of broken waves. A small wave front passes the gauge at $\omega_p t \sim -12$ (i.e. $t \sim -4$ s) before a much larger front at $\omega_p t \sim -7.5$ (i.e. $t \sim -2.5$ s). Thus, the optimal runup (for this beach slope and wave amplitude) appears to require phase/focus location shifts that generate one large bore at the SWS, with relatively small precursor waves to minimise momentum losses from the downrushing flow.

Noting the similarity of the time-shifted records at the beach toe, it may be assumed that the optimisation of runup for a particular focus location may be achieved by manipulating the wave phase and focus location to generate a profile resembling a trough-focused wave at the beach toe. Given that a focus location shift causes different phase shifts for the different frequencies within the focused wave group, these $k_i \Delta x$ shifts cannot be perfectly balanced by applying a $\Delta\phi$ shift to all of the frequencies (except in the shallow water limit). Although the waves become less frequency dispersive with decreasing depth, Figure 8 indicates that reasonable agreement between the wave groups at the beach toe will lead to similar agreement in the measured runup time series. For the intermediate-depth kD value used in this study, frequency dispersion remains the dominant process governing the wave transformations offshore of the beach toe.

Detuned cases leading to minimum runup elevations are next investigated. Figure 9 shows the nondimensional free surface elevation time series at the beach toe and SWS, and the runup time series for three detuned cases with $A = 0.0855$ m. Table 2 indicates that the required phase shift from maximum to minimum runup is not 180°. However, the free surface elevation time history at the beach toe does resemble a crest-focused wave group for these detuned cases. The SWS gauge data contain two reasonably large bores, as opposed to the small bore preceding a very

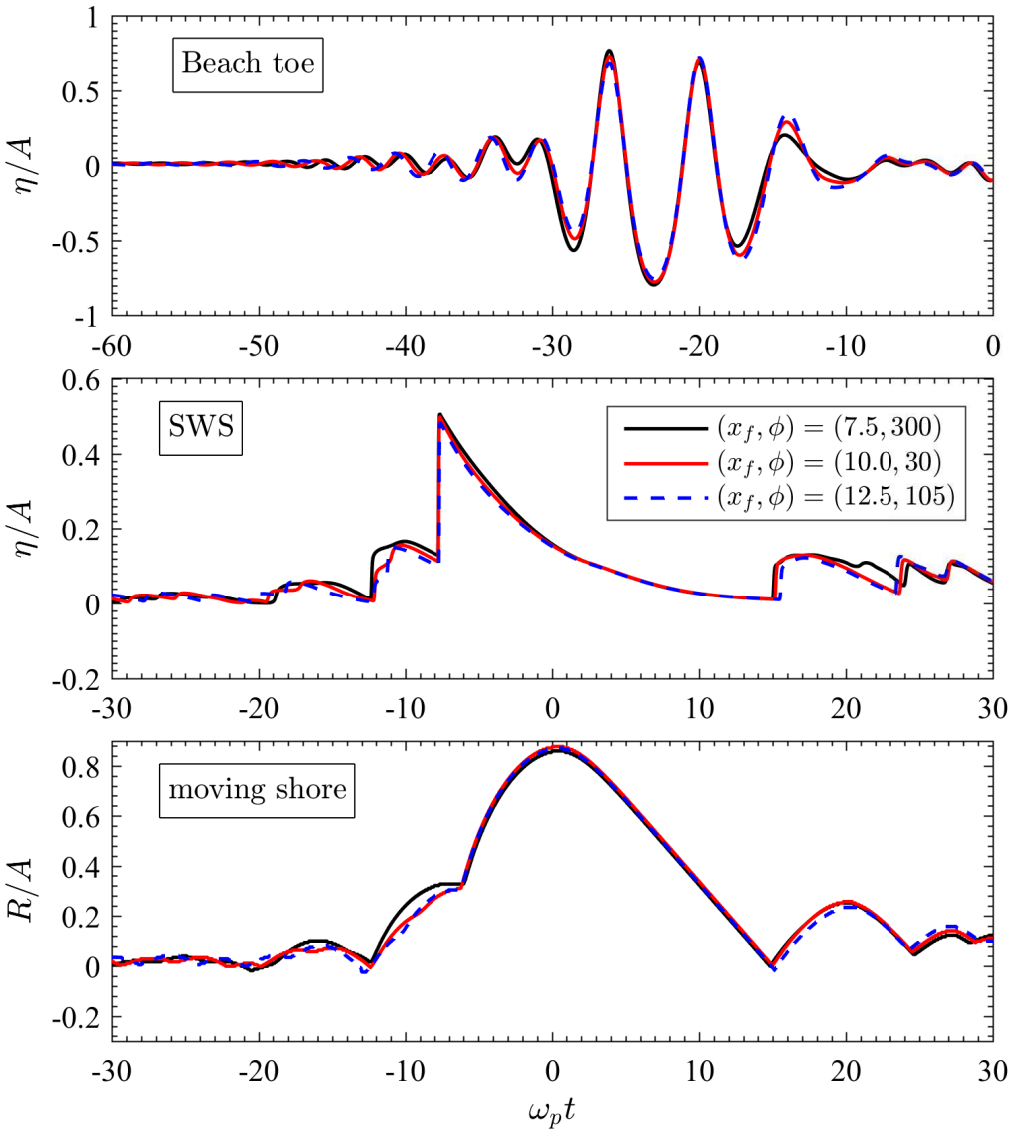

Figure 8: Nondimensional free surface elevation and shoreline motion time series for the three phase/focus location combinations leading to the *maximum* runup for a focused wave group with $A = 0.0855$ m.

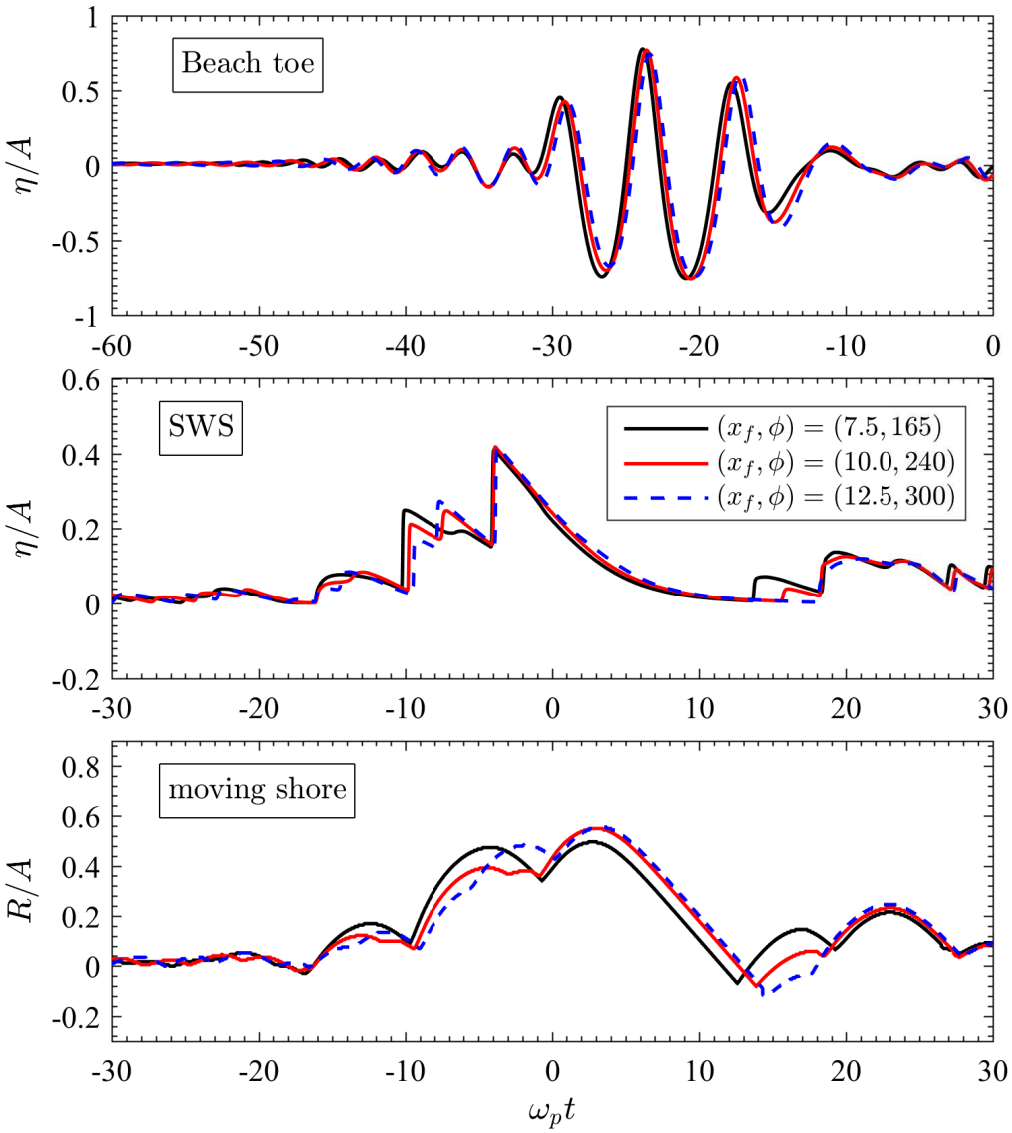

Figure 9: Nondimensional free surface elevation and shoreline motion time series for three phase/focus location combinations leading to the *minimum* runup for a focused wave group with $A = 0.0855$ m.

large bore for the optimal cases. The reduced runup may therefore be caused by momentum losses from the downrush of the first bore. This indicates that the maximum runup may be achieved by maximising the amplitude of a particular bore while minimising the amplitude of the immediately preceding bore.

5.2. Optimisation of runup using second-order wave generation

Having established the conditions leading to the maximum and minimum runup elevations on the plane beach, we now consider the variation of the maximum runup elevation observed in each experiment over the entire parameter space. Figure 10 illustrates the dependence of the maximum (nondimensional) runup on the focus location (x-axis) and phase at focus (y-axis) for focused wave groups of amplitude varying from 0.0285 m to 0.114 m. Focus locations are expressed relative to the beach toe for clarity (with the dashed line representing the SWS location). The results are plotted for phases between $\phi = -360^\circ$ and $\phi = 360^\circ$ to emphasise the periodicity of the runup maxima over the parameter space. Both experimental and numerical runup maxima are plotted using the same colour scale, to highlight the similarities and differences between the predicted and measured runup maxima. The laboratory measurements of runup maxima are relatively sparse in x_f, which created some issues when using a standard contour plot. Since the parametric dependence of the experimental runup maxima was qualitatively very similar to that of the numerical maxima (despite the differences in the maximum amplitude clearly visible in Figure 10), these numerical values were used to determine the expected values of the measured runup maxima at intermediate focus locations (where only numerical values were available). Thus, the experimental contours are plotted as a continuous surface that is constrained to the discrete experimental results (where available) and the scaled numerical predictions at intermediate values. Both experimental and numerical contours were subsequently smoothed by interpolating the results onto a finer grid ($\Delta x_f = 0.05$ m, $\Delta\phi = 5^\circ$) using (constrained) cubic splines. The runup maxima follow diagonal lines (or 'stripes') over the parameter space, with a clear wrap-around at phase multiples of 360°. Thus, for each wave group amplitude there is a band of optimal phase-focus location combinations that correspond to maximum runup. As the focus location is moved inshore (x_f increases), the phase required to generate the maximum runup decreases. Increasing the amplitude moves these optimised colour bands slightly to the right, so that the optimal focus location moves further up the beach. At each amplitude/focus location combination there is a single optimal phase that produces the maximum runup. Note that the phase producing the minimum runup is not necessarily 180° out of phase with the

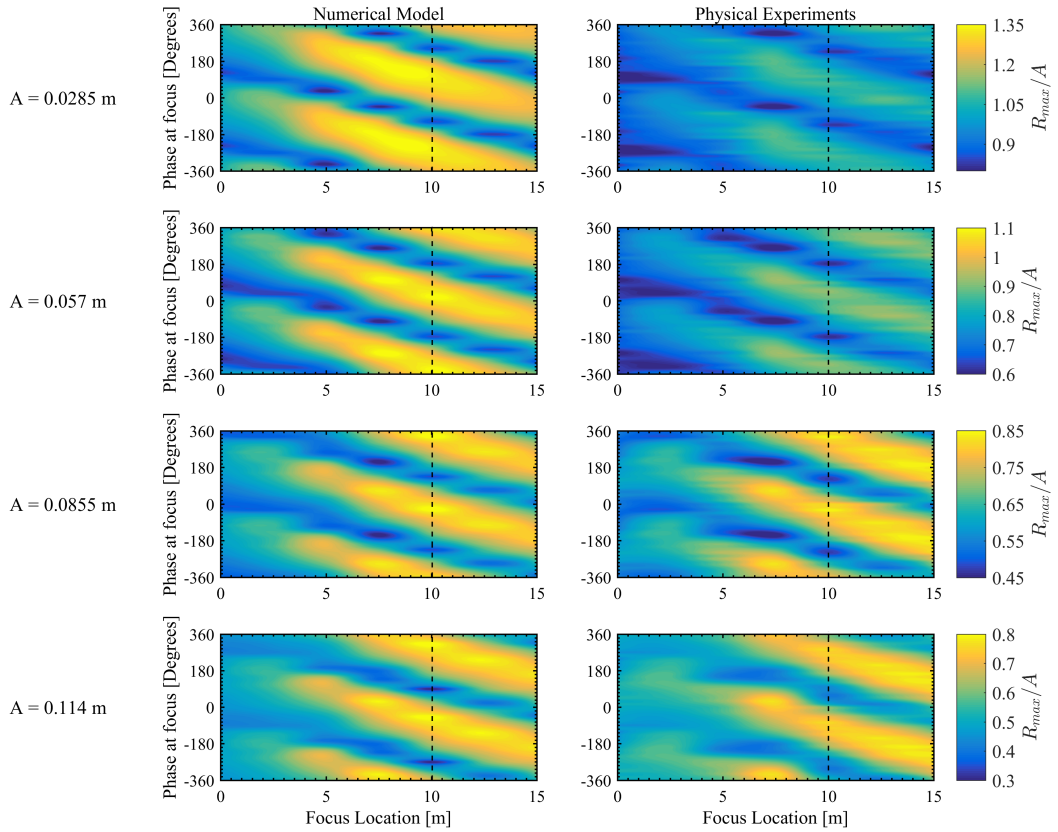

Figure 10: Variation in nondimensional experimental and numerical maximum runup over the range of focus locations, phases (at focus) and amplitudes tested. The left plots are numerical model predictions; the right plots are experimental measurements.

optimal phase. The optimal phase for each focus location also increases slightly with increasing focused wave amplitude. Since an increase in amplitude will lead to an increase in wave steepness (for a given peak frequency), this phase shift may be caused by the earlier onset of breaking of the larger-amplitude waves.

Although the phase and focus-location dependence of the experimental and numerical runup maxima (discussed below) are very similar, the magnitude of the maximum experimental and numerical runup elevations differs over the entire parameter space. At the lowest amplitudes, the predicted maximum runup was consistently larger than measured, partly due to surface tension effects. The reverse was the case at larger amplitude, with the predicted maximum runup at

$A = 0.114$ m less than the measured value, partly because of the incomplete removal of spurious second-order long error waves in the laboratory tests (see Orszaghova et al., 2014). The nondimensional runup decreases with increasing linear wave amplitude, implying that breaking-induced energy losses become more severe with increasing incident wave amplitude (hence steepness). This supports the possibility of saturation of the runup generated by focused wave groups.

5.3. Effect of sub-harmonic error wave on runup optimisation

Orszaghova et al. (2014) used the coupled Boussinesq-nonlinear shallow water equation solver of Orszaghova et al. (2012) to determine the effects of first- and second-order wave generation on the runup of a focused wave group on a plane beach. Orszaghova et al. found that the super-harmonic error waves propagated more slowly than the focused wave group, thus making negligible contribution to runup. However, the sub-harmonic error wave propagated ahead of the focused group as a hump, and acted as a wave setup when the focused group reached the beach. This setup greatly enhanced the ability of the focused wave group to penetrate inshore, thus increasing maximum runup elevation. Here, in addition to considering the effects of linear, partial, and full second-order wave generation on the maximum focused wave group runup, we investigate whether the long error wave alters the phase and focus location dependences of the runup maxima.

Figure 11 shows the experimentally measured maximum (nondimensional) runup of a focused wave group of linear amplitude $A = 0.0855$ m, generated using a first-order and (partial) second-order corrected signal. It should be noted that this amplitude was associated with the optimal model performance, as shown in Figure 10. The use of a first-order paddle signal significantly increased all the maximum runup elevations recorded. The first-order paddle signal also caused a small negative shift in the optimal phase required to generate maximum runup at each focus location, in contrast to the positive shift associated with an increase in the amplitude A (attributed to wave breaking in Section 5.2). This indicates that the long wavelength of the hump of water comprising the leading part of the error wave (shown in Figure 3) can delay the onset of wave breaking, consistent with the analogy of wave setup at the beach. These results are also consistent with the results of Sriram et al. (2015), who found that sub-harmonic error waves caused an onshore shift of the focus location.

Clearly, use of a first-order wavemaker signal has significantly increased the maximum runup elevations recorded for an incident focused wave amplitude of $A = 0.0855$ m, even when compared to the imperfect second-order corrections used in the physical experiments (discussed in Section

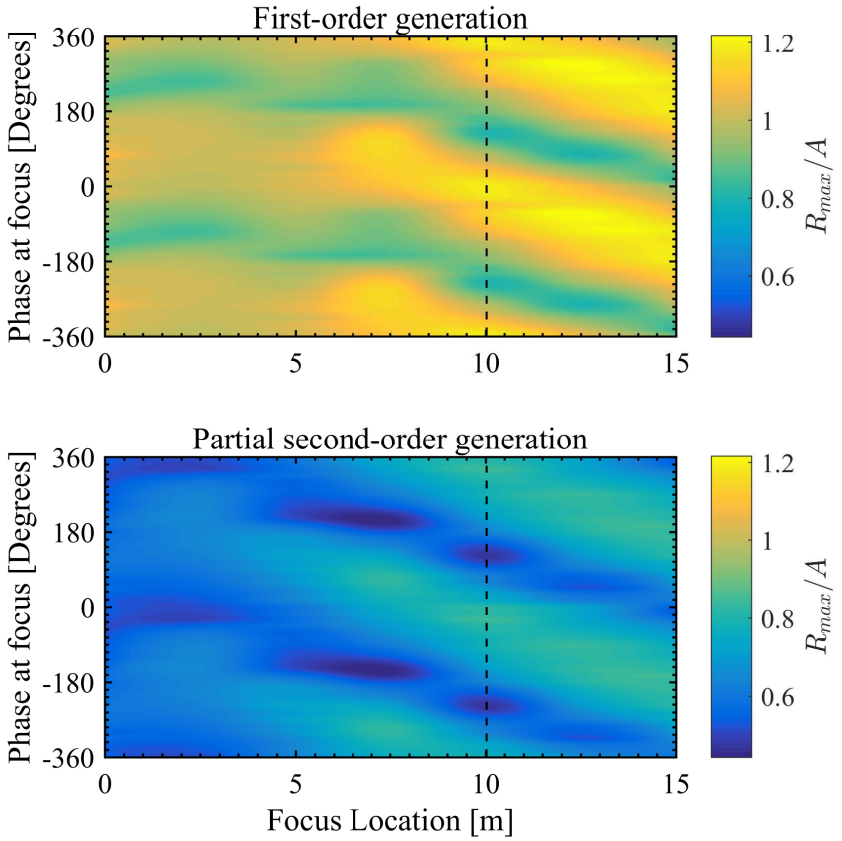

Figure 11: Effect of first- and (partial) second-order wave generation on the experimentally measured maximum runup elevation for a focused wave group of linear amplitude $A = 0.0855$ m, where the runup has been nondimensionalised by A.

2). The experimental results obtained using first-order wave generation were compromised by the sub-harmonic error wave. This implies that other experimental (or numerical, see Orszaghova et al., 2014) studies using linear wave generation will significantly over-estimate the maximum runup. Empirical relationships based on such studies may also over-estimate extreme runup elevations.

5.4. Amplitude dependence of focused wave runup

Figure 10 indicates that certain combinations of phase and focus location within the band of optimal values will generate maximum runup for a linear-focused wave group. The otherwise infinite range of predicted focus location is constrained by the offshore location of the wavemaker and the onshore flume boundary in practice. However, as discussed by Orszaghova (2011), runup maxima are unlikely to be generated by focus locations great distances onshore or offshore of those tested in this study owing to dispersion of the wave group (whether pre- or post-breaking). Thus, the maximum runup attained for the linear focus group amplitudes may be considered to be the global maximum for a given wave group amplitude. Although focus locations more than 15 m onshore of the beach toe were not tested, the colour bands of Figure 11 provide confidence that the maximum runup elevations have been captured over the range of amplitudes considered.

Figure 12 shows the measured and predicted optimised wave runups as functions of linear wave group amplitude at focus in nondimensional form. The optimised runup and (linear) focused wave group amplitudes are nondimensionalised by the offshore water depth, $D = 0.5$ m. Effects of first-order and full second-order wave generation on the simulated runup are also shown. Since the sub-harmonic error wave amplitude increases as the linear focused wave amplitude squared, this error wave dominates the optimised runup at larger linear amplitudes. All investigations of extreme coastal responses using first-order wave generation are affected by this error wave, but to varying extent (depending on the degree of nonlinearity of the waves being generated). Other discrepancies between the experimental and numerical optimised runup curves may be partly attributed to surface tension effects (at lower amplitudes) and incomplete removal of the sub-harmonic error wave (more prominent at higher amplitudes).

For numerical simulations, the optimised runup increases with linear group amplitude. However, wave breaking causes the runup to asymptote at larger amplitudes. A global maximum runup elevation (over all focused wave group amplitudes) could not be identified because the extreme amplitudes required for such a global maximum would violate the weakly nonlinear assumption underpinning the numerical model. However, extreme amplitudes appear to yield ever

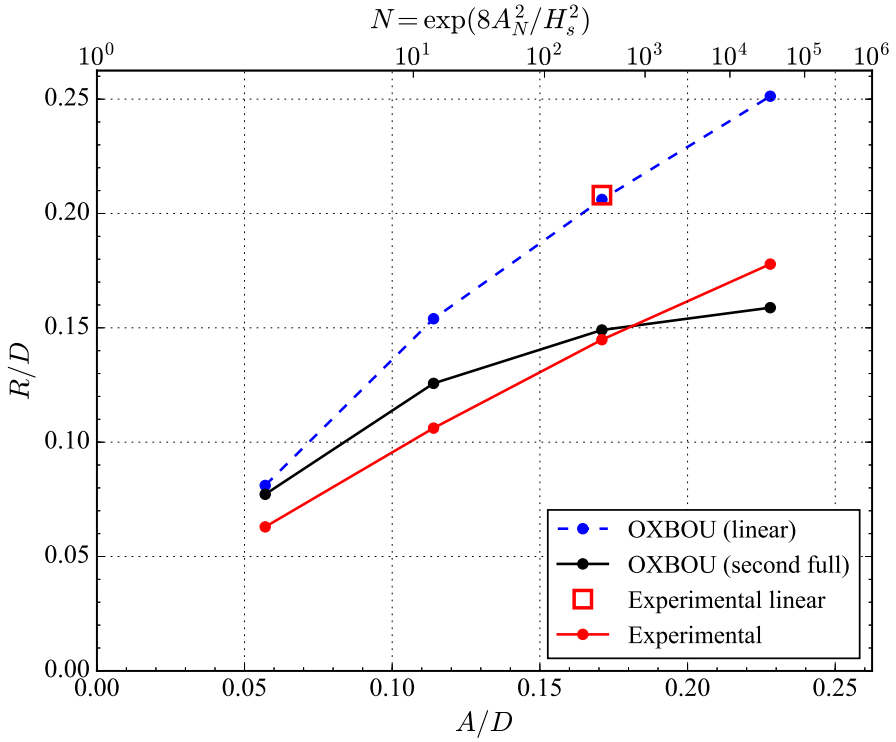

Figure 12: Variation of the measured and predicted optimised (maximum) runup with linear focused wave amplitude for first-order, partial second-order and full second-order wave generation. Variables are presented in nondimensional form, and the upper x axis represents the number of waves N generating the '1 in N' wave amplitude A_N (using $H_s = 0.2$ m).

smaller increases in optimised runup, relying on events with very low occurrence probabilities if translated across into the extreme response to a storm of increasing length but fixed properties (significant wave height and peak period). The occurrence probabilities of a focused wave group with given linear amplitude may be obtained by assuming the following Rayleigh distribution:

$$A_N = \sqrt{2\sigma^2 \ln N}, \tag{3}$$

where A_N is the '1 in N' wave amplitude for a sea state with a variance σ^2. If A_N is the 1 in 1000 wave for a given sea state, then the 1 in 2000 wave would generate an amplitude increase of only about 5%, whereas an order-of-magnitude decrease in probability to the 1 in 10000 wave would generate a 15% increase in A_N. This effect is shown in the upper x axis of Figure 12, where N is the number of waves corresponding to a wave amplitude A_N. It should be noted that the assumed significant wave height used to calculate these N values is $H_s = 0.2$ m. The asymptotic behaviour of maximum runup with increasing amplitude may provide a practical upper bound

on maximum runup generated by a particular sea state (with significant wave height $H_s = 4\sigma$) on a prescribed beach geometry. This is consistent with the saturation of the incident frequency band identified by Raubenheimer and Guza (1996); Stockdon et al. (2006); Senechal et al. (2011). Significantly larger wave runup on the same beach geometry would then require a more severe sea state.

The present discussion is based on results obtained for 1-D wave propagation and runup on an idealised 1 : 20 plane beach. Runup on natural beaches often exhibits significant lateral variation, and depends strongly on the local bathymetry which is usually complicated in the nearshore zone. Moreover, erodible beaches may undergo substantial morphological changes during large storm events. Incident storm waves may also force low frequency infra-gravity waves within the surf zone, which may contribute strongly to the maximum wave runup on the beach. Although not considered in this paper, these effects deserve attention in future studies. The present study has demonstrated that (for the one-dimensional plane beach geometry considered) the runup of focused waves approaches an upper limit in a given sea state of plausible length, which may be useful for the design of coastal defence structures.

6. Conclusions

This paper has described investigations into focused wave group runup on a plane beach using a series of physical experiments and numerical model simulations. It is found that use of a linear paddle signal erroneously increased the maximum runup elevations over the entire parameter space (particularly at the largest amplitudes) and shifted slightly the phase/focus location values leading to maximum runup for a given focused wave group amplitude. Following Orszaghova et al. (2014); Sriram et al. (2015), the present analysis has confirmed that linear generation signals are inappropriate for the investigation of extreme coastal responses, such as runup and overtopping. Any empirical results relying on linear wave generation should be checked accordingly. By appropriately modifying the wavemaker control signal, partial suppression of the sub-harmonic error wave was achieved in the laboratory wave flume. The model was calibrated using linear generation signals by tuning the wave breaking parameter and the friction coefficient, with the best agreement achieved at $A = 0.0855$ m. This calibration also provided confidence in the results of the model when using full second-order correction. The partial long error wave correction appears to be the best that can be achieved using the present EDL two-component wavemaker in the absence of direct displacement control. The nonlinear error correction of this type of laboratory wavemaker is worth further research and development.

The maximum runup generated by a focused wave group exhibited strong dependence on the linear wave group amplitude at focus, focus location, and phase at focus of the wave group. The amplitude of the focused wave group is used to set the probability of occurrence of the incident wave group, which does not depend on phase or focus location. However, the combined dependence implied that the maximum runup of a focused wave group cannot be characterised using significant wave height, spectral shape, or peak frequency alone. For each linear focused wave amplitude, a band of optimal focus locations and phases at focus generated the maximum (or minimum) runup; this band was slightly phase-shifted with increasing amplitude, most likely due to the earlier onset of wave breaking. For the particular incident wave conditions and beach geometry considered here, the results indicated that these optimal phase/focus location combinations may be maintained by attempting to replicate the wave group phasing at the beach toe.

Over the range of tests conducted, the maximum runup of a linear focused wave group of prescribed amplitude was obtained for a single phase and focus location combination (within the optimal band). As the incident focused wave group amplitude increased, wave breaking became more important, occurring further offshore, and the maximum runup elevation began to exhibit asymptotic behaviour. Since the sub-harmonic error wave increased as the square of the amplitude of the linear focused wave group, failure to remove this error wave prevented the maximum runup from approaching an upper limit. Although an absolute maximum runup elevation was not reached during the present study, use of Rayleigh statistics indicated that the focused wave runup (for a given sea state defined by its spectral shape, peak frequency and significant wave height) may reach a practical upper limit with a very low exceedance probability. This may have implications for the design of coastal structures, offering an alternative to lengthy simulations in the calculation of extreme coastal responses and complementing existing empirical methods.

Acknowledgements

This work was conducted within the ENFORCE (Extreme Responses using NewWave: Forces, Overtopping and Runup in Coastal Engineering) project, under EPSRC Grant EP/K024108/1.

References

Almar, R., Catalán, P., Ibaceta, R., Blenkinsopp, C., Cienfuegos, R., Villagrán, M., Aguilera, J.C., Castelle, B., 2014. Swash zone based reflection during energetic wave conditions at a dissipative beach: Toward a wave-by-wave approach. Coastal Engineering Proceedings 1, 34.

Almeida, L.P., Masselink, G., Russell, P., Davidson, M., Poate, T., McCall, R., Blenkinsopp, C., Turner, I., 2013. Observations of the swash zone on a gravel beach during a storm using a laser-scanner (Lidar). Journal of Coastal Research , 636–641URL: http://dx.doi.org/10.2112/SI65-108.1, doi:10.2112/SI65-108.1. special Issue No. 65.

Bai, W., Eatock Taylor, R., 2006. Higher-order boundary element simulation of fully nonlinear wave radiation by oscillating vertical cylinders. Appl. Ocean Res. 28, 247–265.

Bai, W., Eatock Taylor, R., 2007. Numerical simulation of fully nonlinear regular and focused wave diffraction around a vertical cylinder using domain decomposition. Appl. Ocean Res. 29, 55–71.

Baldock, T., Holmes, P., Horn, D., 1997. Low frequency swash motion induced by wave grouping. Coastal Engineering 32, 197 – 222. URL: http://www.sciencedirect.com/science/article/pii/S0378383997817504, doi:http://dx.doi.org/10.1016/S0378-3839(97)81750-4.

Baldock, T.E., Swan, C., Taylor, P.H., 1996. A laboratory study of nonlinear surface waves on water. Philosophical Transactions of the Royal Society of London A: Mathematical, Physical and Engineering Sciences 354, 649–676. URL: http://rsta.royalsocietypublishing.org/content/354/1707/649, doi:10.1098/rsta.1996.0022, arXiv:http://rsta.royalsocietypublishing.org/content/354/1707/649.full.pdf.

Bateman, W., Swan, C., Taylor, P., 2001. On the efficient numerical simulation of directionally spread surface water waves. Journal of Computational Physics 174, 277 – 305. URL: http://www.sciencedirect.com/science/article/pii/S0021999101969062, doi:http://dx.doi.org/10.1006/jcph.2001.6906.

Battjes, J.A., 1974. Surf similarity, American Society of Civil Engineers. pp. 466–480.

Blenkinsopp, C., Matias, A., Howe, D., Castelle, B., Marieu, V., Turner, I., 2016. Wave runup and overwash on a prototype-scale sand barrier. Coastal Engineering 113, 88 – 103. URL:

http://www.sciencedirect.com/science/article/pii/S0378383915001362, doi:http://dx.doi.org/10.1016/j.coastaleng.2015.08.006. barrier Dynamics Experiment II: sediment processes across a large-scale sand barrier.

Blenkinsopp, C., Mole, M., Turner, I., Peirson, W., 2010. Measurements of the time-varying free-surface profile across the swash zone obtained using an industrial LIDAR. Coastal Engineering 57, 1059–1065.

Blenkinsopp, C.E., Turner, I.L., Allis, M.J., Peirson, W.L., Garden, L.E., 2012. Application of LiDAR technology for measurement of time-varying free-surface profiles in a laboratory wave flume. Coastal Engineering 68, 1 – 5. URL: http://www.sciencedirect.com/science/article/pii/S0378383912000762, doi:http://dx.doi.org/10.1016/j.coastaleng.2012.04.006.

Borthwick, A.G.L., Hunt, A.C., Feng, T., Taylor, P.H., Stansby, P.K., 2006. Flow kinematics of focused wave groups on a plane beach in the U.K. Coastal Research Facility. Coastal Engineering 53, 1033 – 1044. doi:http://dx.doi.org/10.1016/j.coastaleng.2006.06.007.

Brocchini, M., Baldock, T.E., 2008. Recent advances in modeling swash zone dynamics: Influence of surf-swash interaction on nearshore hydrodynamics and morphodynamics. Reviews of Geophysics 46, 1–21. doi:10.1029/2006RG000215.

Dickson, M.E., Walkden, M.J.A., Hall, J.W., 2007. Systemic impacts of climate change on an eroding coastal region over the twenty-first century. Climatic Change 84, 141–166. URL: http://dx.doi.org/10.1007/s10584-006-9200-9, doi:10.1007/s10584-006-9200-9.

Erduran, K.S., Ilic, S., Kutija, V., 2005. Hybrid finite-volume finite-difference scheme for the solution of Boussinesq equations. International Journal for Numerical Methods in Fluids 49, 1213–1232. URL: http://dx.doi.org/10.1002/fld.1021, doi:10.1002/fld.1021.

Erikson, L., Larson, M., Hanson, H., 2005. Prediction of swash motion and run-up including the effects of swash interaction. Coastal Engineering 52, 285–302.

Fiedler, J.W., Brodie, K.L., McNinch, J.E., Guza, R.T., 2015. Observations of runup and energy flux on a low-slope beach with high-energy, long-period ocean swell. Geophysical Research Letters 42, 9933–9941. URL: http://dx.doi.org/10.1002/2015GL066124, doi:10.1002/2015GL066124. 2015GL066124.

Fitzgerald, C.J., Taylor, P.H., Taylor, R.E., Grice, J., Zang, J., 2014. Phase manipulation and the harmonic components of ringing forces on a surface-piercing column. Proceedings of the Royal Society of London A: Mathematical, Physical and Engineering Sciences 470. doi:10.1098/rspa.2013.0847.

Gibson, R., Swan, C., 2007. The evolution of large ocean waves: the role of local and rapid spectral changes. Proceedings of the Royal Society of London A: Mathematical, Physical and Engineering Sciences 463, 21–48. URL: http://rspa.royalsocietypublishing.org/content/463/2077/21, doi:10.1098/rspa.2006.1729, arXiv:http://rspa.royalsocietypublishing.org/content/463/2077/21.full.pdf.

Guza, R.T., Feddersen, F., 2012. Effect of wave frequency and directional spread on shoreline runup. Geophysical Research Letters 39, 1–5. doi:10.1029/2012GL051959.

Guza, R.T., Thornton, E.B., 1982. Swash oscillations on a natural beach. Journal of Geophysical Research: Oceans 87, 483–491. URL: http://dx.doi.org/10.1029/JC087iC01p00483, doi:10.1029/JC087iC01p00483.

Hall, J.W., Sayers, P.B., Walkden, M.J., Panzeri, M., 2006. Impacts of climate change on coastal flood risk in England and Wales: 2030–2100. Philosophical Transactions of the Royal Society of London A: Mathematical, Physical and Engineering Sciences 364, 1027–1049. URL: http://rsta.royalsocietypublishing.org/content/364/1841/1027, doi:10.1098/rsta.2006.1752, arXiv:http://rsta.royalsocietypublishing.org/content/364/1841/1027.full.pdf.

Hedges, T.S., Mase, H., 2004. Modified Hunt's equation incorporating wave setup. Journal of Waterway, Port, Coastal, and Ocean Engineering 130, 109–113. URL: http://dx.doi.org/10.1061/(ASCE)0733-950X(2004)130:3(109), doi:10.1061/(ASCE)0733-950X(2004)130:3(109), arXiv:http://dx.doi.org/10.1061/(ASCE)0733-950X(2004)130:3(109).

Higuera, P., Lara, J.L., Losada, I.J., 2013. Simulating coastal engineering processes with OpenFOAM®. Coastal Engineering 71, 119–134.

Higuera, P., Losada, I.J., Lara, J.L., 2015. Three-dimensional numerical wave generation with moving boundaries. Coastal Engineering 101, 35 – 47. doi:http://dx.doi.org/10.1016/j.coastaleng.2015.04.003.

Hofland, B., Wenneker, I., Van Steeg, P., 2014. Short test durations for wave overtopping experiments, in: Proceedings of the 5th International Conference on the Application of Physical Modelling to Port and Coastal Protection, Varna, Bulgaria. pp. 349–358.

Holland, K., Raubenheimer, B., Guza, R., Holman, R.A., 1995. Runup kinematics on a natural beach. Journal of Geophysical Research: Oceans (1978–2012) 100, 4985–4993.

Holman, R., 1986. Extreme value statistics for wave run-up on a natural beach. Coastal Engineering 9, 527 – 544. URL: http://www.sciencedirect.com/science/article/pii/0378383986900025, doi:http://dx.doi.org/10.1016/0378-3839(86)90002-5.

Holman, R., Haller, M.C., 2013. Remote sensing of the nearshore. Annual Review of Marine Science 5, 95–113. URL: http://dx.doi.org/10.1146/annurev-marine-121211-172408, doi:10.1146/annurev-marine-121211-172408, arXiv:http://dx.doi.org/10.1146/annurev-marine-121211-172408. pMID: 22809186.

Holman, R.A., Sallenger, A.H., 1985. Setup and swash on a natural beach. Journal of Geophysical Research: Oceans 90, 945–953. URL: http://dx.doi.org/10.1029/JC090iC01p00945, doi:10.1029/JC090iC01p00945.

Hughes, M.G., Aagaard, T., Baldock, T.E., Power, H.E., 2014. Spectral signatures for swash on reflective, intermediate and dissipative beaches. Marine Geology 355, 88–97.

Hughes, M.G., Moseley, A.S., 2007. Hydrokinematic regions within the swash zone. Continental Shelf Research 27, 2000 – 2013. URL: http://www.sciencedirect.com/science/article/pii/S0278434307001288, doi:http://dx.doi.org/10.1016/j.csr.2007.04.005.

Hughes, M.G., Moseley, A.S., Baldock, T.E., 2010. Probability distributions for wave runup on beaches. Coastal Engineering 57, 575–584.

Hughes, S.A., 2004. Estimation of wave run-up on smooth, impermeable slopes using the wave momentum flux parameter. Coastal Engineering 51, 1085 – 1104. URL: http://www.sciencedirect.com/science/article/pii/S0378383904000985, doi:http://dx.doi.org/10.1016/j.coastaleng.2004.07.026.

Hunt, A., 2003. Extreme waves, overtopping and flooding at sea defences. D.Phil.. University of Oxford (United Kingdom).

Hunt, I.A., 1959. Design of seawalls and breakwaters. Journal of the Waterways and Harbors Division 85, 123–152.

Hunt-Raby, A.C., Borthwick, A., Stansby, P.K., Taylor, P.H., 2011. Experimental measurement of focused wave group and solitary wave overtopping. Journal of Hydraulic Research 49, 450–464. doi:10.1080/00221686.2010.542616.

ICE, U.K., 2014. The state of the nation: Infrastructure 2014 , 28.

Johannessen, T., Swan, C., 1997. Nonlinear transient water waves—part I. A numerical method of computation with comparisons to 2-D laboratory data. Applied Ocean Research 19, 293 – 308. URL: http://www.sciencedirect.com/science/article/pii/S0141118797000370, doi:http://dx.doi.org/10.1016/S0141-1187(97)00037-0.

Johannessen, T., Swan, C., 2001. A laboratory study of the focusing of transient and directionally spread surface water waves. Proceedings of the Royal Society of London A: Mathematical, Physical and Engineering Sciences 457, 971–1006. URL: http://rspa.royalsocietypublishing.org/content/457/2008/971, doi:10.1098/rspa.2000.0702, arXiv:http://rspa.royalsocietypublishing.org/content/457/2008/971.full.pdf.

Jonathan, P., Taylor, P.H., 1997. On irregular, nonlinear waves in a spread sea. Journal of Offshore Mechanics and Arctic Engineering 119, 37–41. 10.1115/1.2829043.

Kharif, C., Pelinovsky, E., 2003. Physical mechanisms of the rogue wave phenomenon. European Journal of Mechanics - B/Fluids 22, 603 – 634. URL: http://www.sciencedirect.com/science/article/pii/S0997754603000724, doi:http://dx.doi.org/10.1016/j.euromechflu.2003.09.002.

Kobayashi, N., 1999. Wave runup and overtopping on beaches and coastal structures, in: Liu, P. (Ed.), Advances in Coastal Engineering. World Scientific.

Kobayashi, N., Wurjanto, A., 1992. Irregular wave setup and run?up on beaches. Journal of Waterway, Port, Coastal, and Ocean Engineering 118, 368–386. URL: http://dx.doi.org/10.1061/(ASCE)0733-950X(1992)118:4(368), doi:10.1061/(ASCE)0733-950X(1992)118:4(368), arXiv:http://dx.doi.org/10.1061/(ASCE)0733-950X(1992)118:4(368).

Kraus, N.C., Smith, J.M., Sollitt, C.K., 1994. SUPERTANK Laboratory data collection project, Volume 1: Main text. Technical Report CERC-94-3. U.S. Army Engineering Waterways Experiment Station, Coastal Engineering Research Center. Vicksburg, Mississippi.

Longuet-Higgins, M.S., Stewart, R., 1960. Changes in the form of short gravity waves on long waves and tidal currents. Journal of Fluid Mechanics 8, 565–583.

Mase, H., 1989. Random wave runup height on gentle slope. Journal of Waterway, Port, Coastal, and Ocean Engineering 115, 649–661. URL: http://dx.doi.org/10.1061/(ASCE)0733-950X(1989)115:5(649), doi:10.1061/(ASCE)0733-950X(1989)115:5(649), arXiv:http://dx.doi.org/10.1061/(ASCE)0733-950X(1989)115:5(649).

Mase, H., Iwagaki, Y., 1984. Run-up of random waves on gentle slopes. Coastal Engineeering Proceedings 1. URL: https://icce-ojs-tamu.tdl.org/icce/index.php/icce/article/view/382. issn: 2156-1028.

Masselink, G., Ruju, A., Conley, D., Turner, I., Ruessink, G., Matias, A., Thompson, C., Castelle, B., Puleo, J., Citerone, V., Wolters, G., 2016. Large-scale barrier dynamics experiment {II} (BARDEX II): Experimental design, instrumentation, test program, and data set. Coastal Engineering 113, 3 – 18. URL: http://www.sciencedirect.com/science/article/pii/S0378383915001295, doi:http://dx.doi.org/10.1016/j.coastaleng.2015.07.009. barrier Dynamics Experiment II: sediment processes across a large-scale sand barrier.

Nielsen, P., Hanslow, D.J., 1991. Wave runup distributions on natural beaches. Journal of Coastal Research 7, 1139–1152. URL: http://www.jstor.org/stable/4297933.

Orszaghova, J., 2011. Solitary waves and wave groups at the shore. D.Phil.. University of Oxford (United Kingdom). URL: http://ora.ox.ac.uk/objects/uuid:5b168bdc-4956-4152-a303-b23a6067bf42.

Orszaghova, J., Borthwick, A.G.L., Taylor, P.H., 2012. From the paddle to the beach - a Boussinesq shallow water numerical wave tank based on Madsen and Sorensen's equations. Journal of Computational Physics 231, 328 – 344. doi:http://dx.doi.org/10.1016/j.jcp.2011.08.028.

Orszaghova, J., Taylor, P.H., Borthwick, A.G.L., Raby, A.C., 2014. Importance of second-order wave generation for focused wave group run-up and overtopping. Coastal Engineering 94, 63 – 79. doi:http://dx.doi.org/10.1016/j.coastaleng.2014.08.007.

Park, H., Cox, D.T., 2016. Empirical wave run-up formula for wave, storm surge and berm width. Coastal Engineering 115, 67 – 78. URL: http://www.sciencedirect.com/science/

article/pii/S0378383915001830, doi:http://dx.doi.org/10.1016/j.coastaleng.2015.10.006. swash-zone Processes.

Penland, S., Connor Jr, P.F., Beall, A., Fearnley, S., Williams, S.J., 2005. Changes in Louisiana's shoreline: 1855–2002. Journal of Coastal Research , 7–39.

Pullen, T., Allsop, N.W.H., Bruce, T., Kortenhaus, A., Schüttrumpf, H., Van der Meer, J.W., 2007. EurOtop, European Overtopping Manual – Wave Overtopping of Sea Defences and Related Structures: Assessment Manual. Technical Report. Environmental Agency, UK, Expertise Netwerk Waterkeren, NL, and Kuratorium f´ur Forschung im K´usteningenieurwesen, DE. URL: http://www.overtopping-manual.com/eurotop.pdf.

Raubenheimer, B., Guza, R.T., 1996. Observations and predictions of run-up. Journal of Geophysical Research: Oceans 101, 25575–25587. URL: http://dx.doi.org/10.1029/96JC02432, doi:10.1029/96JC02432.

Raubenheimer, B., Guza, R.T., Elgar, S., Kobayashi, N., 1995. Swash on a gently sloping beach. Journal of Geophysical Research: Oceans 100, 8751–8760. URL: http://dx.doi.org/10.1029/95JC00232, doi:10.1029/95JC00232.

Ruessink, B.G., Kleinhans, M.G., van den Beukel, P.G.L., 1998. Observations of swash under highly dissipative conditions. Journal of Geophysical Research: Oceans 103, 3111–3118. URL: http://dx.doi.org/10.1029/97JC02791, doi:10.1029/97JC02791.

Ruggiero, P., 2013. Is the intensifying wave climate of the U.S. Pacific Northwest increasing flooding and erosion risk faster than sea-level rise? Journal of Waterway, Port, Coastal, and Ocean Engineering 139, 88–97. URL: http://dx.doi.org/10.1061/(ASCE)WW.1943-5460.0000172, doi:10.1061/(ASCE)WW.1943-5460.0000172.

Ruggiero, P., Komar, P.D., McDougal, W.G., Marra, J.J., Beach, R.A., 2001. Wave runup, extreme water levels and the erosion of properties backing beaches. Journal of Coastal Research 17, 407–419. URL: http://www.jstor.org/stable/4300192.

Schäffer, H.A., 1996. Second-order wavemaker theory for irregular waves. Ocean Engineering 23, 47 – 88. doi:http://dx.doi.org/10.1016/0029-8018(95)00013-B.

Senechal, N., Coco, G., Bryan, K.R., Holman, R.A., 2011. Wave runup during extreme storm conditions. Journal of Geophysical Research: Oceans 116, n/a–n/a. URL: http://dx.doi.org/10.1029/2010JC006819, doi:10.1029/2010JC006819. c07032.

Sharma, J.N., Dean, R.G., 1981. Second-order directional seas and associated wave forces. Society of Petroleum Engineers Journal 21, 129–140. doi:http://dx.doi.org/10.2118/8584-PA.

Shi, F., Kirby, J.T., Harris, J.C., Geiman, J.D., Grilli, S.T., 2012. A high-order adaptive time-stepping {TVD} solver for Boussinesq modeling of breaking waves and coastal inundation. Ocean Modelling 43–44, 36 – 51. URL: http://www.sciencedirect.com/science/article/pii/S1463500311002010, doi:http://dx.doi.org/10.1016/j.ocemod.2011.12.004.

Smith, S., Swan, C., 2002. Extreme two-dimensional water waves: an assessment of potential design solutions. Ocean Engineering 29, 387 – 416. URL: http://www.sciencedirect.com/science/article/pii/S0029801801000282, doi:http://dx.doi.org/10.1016/S0029-8018(01)00028-2.

Soldini, L., Antuono, M., Brocchini, M., 2013. Numerical modeling of the influence of the beach profile on wave run-up. Journal of Waterway, Port, Coastal, and Ocean Engineering 139, 61–71. URL: http://dx.doi.org/10.1061/(ASCE)WW.1943-5460.0000163, doi:10.1061/(ASCE)WW.1943-5460.0000163, arXiv:http://dx.doi.org/10.1061/(ASCE)WW.1943-5460.0000163.

Spinneken, J., Swan, C., 2009a. Second-order wave maker theory using force-feedback control. Part I: A new theory for regular wave generation. Ocean Engineering 36, 539 – 548. doi:http://dx.doi.org/10.1016/j.oceaneng.2009.01.019.

Spinneken, J., Swan, C., 2009b. Second-order wave maker theory using force-feedback control. Part II: An experimental verification of regular wave generation. Ocean Engineering 36, 549 – 555. doi:http://dx.doi.org/10.1016/j.oceaneng.2009.01.007.

Sriram, V., Schlurmann, T., Schimmels, S., 2015. Focused wave evolution using linear and second order wavemaker theory. Applied Ocean Research 53, 279 – 296. URL: http://www.sciencedirect.com/science/article/pii/S0141118715001212, doi:http://dx.doi.org/10.1016/j.apor.2015.09.007.

Stockdon, H.F., Holman, R.A., Howd, P.A., Jr., A.H.S., 2006. Empirical parameterization of setup, swash, and runup. Coastal Engineering 53, 573 – 588. URL: http://www.sciencedirect.com/science/article/pii/S0378383906000044, doi:http://dx.doi.org/10.1016/j.coastaleng.2005.12.005.

Sutherland, J., Gouldby, B., 2003. Vulnerability of coastal defences to climate change. Proceedings of the Institution of Civil Engineers - Water and Maritime Engineering 156, 137–145. URL: http://www.icevirtuallibrary.com/doi/abs/10.1680/wame.2003.156.2.137, doi:10.1680/wame.2003.156.2.137.

Taylor, P.H., Williams, B.A., 2004. Wave statistics for intermediate depth water - NewWaves and symmetry. Journal of Offshore Mechanics and Arctic Engineering 126, 54–59. 10.1115/1.1641796.

Thornton, E.B., Guza, R.T., 1983. Transformation of wave height distribution. Journal of Geophysical Research: Oceans 88, 5925–5938. URL: http://dx.doi.org/10.1029/JC088iC10p05925, doi:10.1029/JC088iC10p05925.

Tissier, M., Bonneton, P., Marche, F., Chazel, F., Lannes, D., 2012. A new approach to handle wave breaking in fully non-linear Boussinesq models. Coastal Engineering 67, 54 – 66. URL: http://www.sciencedirect.com/science/article/pii/S0378383912000749, doi:http://dx.doi.org/10.1016/j.coastaleng.2012.04.004.

Toffoli, A., Gramstad, O., Trulsen, K., Monbaliu, J., Bitner-Gregersen, E., Onorato, M., 2010. Evolution of weakly nonlinear random directional waves: laboratory experiments and numerical simulations. Journal of Fluid Mechanics 664, 313–336.

Tonelli, M., Petti, M., 2012. Shock-capturing Boussinesq model for irregular wave propagation. Coastal Engineering 61, 8 – 19. URL: http://www.sciencedirect.com/science/article/pii/S0378383911001815, doi:http://dx.doi.org/10.1016/j.coastaleng.2011.11.006.

Tromans, P.S., Anaturk, A.R., Hagemeijer, P., 1991. A new model for the kinematics of large ocean waves - application as a design wave, in: Proceedings of the First International Offshore and Polar Engineering Conference, The International Society of Offshore and Polar Engineers. pp. 64–71.

van der Meer, J.W., Stam, C.M., 1992. Wave runup on smooth and rock slopes of coastal structures. Journal of Waterway, Port, Coastal, and Ocean Engineering 118, 534–550. URL: http://dx.doi.org/10.1061/(ASCE)0733-950X(1992)118:5(534), doi:10.1061/(ASCE)0733-950X(1992)118:5(534), arXiv:http://dx.doi.org/10.1061/(ASCE)0733-950X(1992)118:5(534).

Vousdoukas, M., Velegrakis, A., Dimou, K., Zervakis, V., Conley, D., 2009. Wave run-up observations in microtidal, sediment-starved pocket beaches of the eastern mediterranean. Journal of Marine Systems 78, S37–S47.

Walker, D.A.G., Taylor, P.H., Eatock Taylor, R., 2004. The shape of large surface waves on the open sea and the Draupner New Year wave. Applied Ocean Research 26, 73 – 83. doi:http://dx.doi.org/10.1016/j.apor.2005.02.001.

Whittaker, C.N., Raby, A.C., Fitzgerald, C.J., Taylor, P.H., 2016. The average shape of large waves in the coastal zone. Coastal Engineering 114, 253–264.

Zhang, K., Douglas, B.C., Leatherman, S.P., 2004. Global warming and coastal erosion. Climatic Change 64, 41–58. URL: http://dx.doi.org/10.1023/B:CLIM.0000024690.32682.48, doi:10.1023/B:CLIM.0000024690.32682.48.

LaTeX Source Files

Click here to download LaTeX Source Files: LaTexSourceFiles.zip